Dual-Channel Two-Photon Microscopy Study of Transdermal Transport in Skin Treated with Low-Frequency Ultrasound and a Chemical Enhancer

Joseph Kushner IV[1], Daekeun Kim[2], Peter T.C. So[2], Daniel Blankschtein[1] and Robert S. Langer[1]

Visualization of transdermal permeant pathways is necessary to substantiate model-based conclusions drawn using permeability data. The aim of this investigation was to visualize the transdermal delivery of sulforhodamine B (SRB), a fluorescent hydrophilic permeant, and of rhodamine B hexyl ester (RBHE), a fluorescent hydrophobic permeant, using dual-channel two-photon microscopy (TPM) to better understand the transport pathways and the mechanisms of enhancement in skin treated with low-frequency ultrasound (US) and/or a chemical enhancer (sodium lauryl sulfate – SLS) relative to untreated skin (the control). The results demonstrate that (1) both SRB and RBHE penetrate beyond the stratum corneum and into the viable epidermis only in discrete regions (localized transport regions – LTRs) of US treated and of US/SLS-treated skin, (2) a chemical enhancer is required in the coupling medium during US treatment to obtain two significant levels of increased penetration of SRB and RBHE in US-treated skin relative to untreated skin, and (3) transcellular pathways are present in the LTRs of US treated and of US/SLS-treated skin for SRB and RBHE, and in SLS-treated skin for SRB. In summary, the skin is greatly perturbed in the LTRs of US treated and US/SLS-treated skin with chemical enhancers playing a significant role in US-mediated transdermal drug delivery.

Journal of Investigative Dermatology (2007) **127,** 2832–2846; doi:10.1038/sj.jid.5700908; published online 7 June 2007

INTRODUCTION

Imaging of the skin with two-photon microscopy (TPM) has been offered as an alternative to the use of conventional imaging methods (e.g., scanning electron microscopy, transmission electron microscopy, and confocal fluorescence microscopy) for the investigation of the transdermal transport of both hydrophilic and hydrophobic molecules. TPM is ideal for future *in vivo* applications because it is a non-invasive technique that does not damage the skin (Masters *et al.*, 1998), as is the case for both scanning electron microscopy (Bommannan *et al.*, 1992; Menon *et al.*, 1994; Yamashita *et al.*, 1997; Menon and Elias, 1997) and transmission electron microscopy (Bodde *et al.*, 1991; Paliwal *et al.*, 2006). TPM also provides higher quality images at a greater skin depth compared with confocal microscopy (Denk *et al.*, 1990; Diaspro, 1999; Soeller and Cannell, 1999; Paliwal *et al.*, 2006), because TPM involves three-body collisions (two photons and one fluorescent molecule) to create an excitation event, whereas confocal microscopy involves only two-body collisions (one photon and one fluorescent molecule), which occur with greater frequency (Denk *et al.*, 1990). As a result of the decreased frequency of three-body collisions utilized by TPM, it is possible to better restrict the imaging of fluorophores to the focal plane of interest (Masters *et al.*, 1997; Periasamy *et al.*, 1999), and, therefore, increase the discrimination of the fluorescence signal at increased tissue depths (Denk *et al.*, 1990). The TPM technique has been utilized previously to examine the effect of the chemical enhancer, oleic acid, on the transdermal transport of both a model hydrophilic and a model hydrophobic fluorescent probe – sulforhodamine B (SRB) and rhodamine B hexyl ester (RBHE), respectively (see Table 1 for some relevant physical properties of these probes) (Yu *et al.*, 2001, 2002, 2003a, b).

In a previous investigation, analysis of skin electrical resistivity measurements in the context of the aqueous-pore pathway hypothesis (a theoretical model developed by our group, which relates the permeability of a hydrophilic permeant to the electrical resistivity of the skin through the radii of the aqueous pore channels in the skin; Tang *et al.*, 2001) suggested that transcellular pathways may exist in the stratum corneum of the highly permeable localized transport regions (LTRs, see Figure 1 for example) that are formed in skin treated simultaneously with the chemical enhancer, sodium lauryl sulfate (SLS), and low-frequency ultrasound (US), whereas intercellular pathways were suggested as the

[1]*Department of Chemical Engineering, Massachusetts Institute of Technology, Cambridge, Massachusetts, USA and* [2]*Department of Mechanical Engineering, Massachusetts Institute of Technology, Cambridge, Massachusetts, USA*

Correspondence: Dr Daniel Blankschtein, Department of Chemical Engineering, Massachusetts Institute of Technology, Room 66-444, 77 Massachusetts Avenue, Building 66-257, Cambridge, Massachusetts 02139, USA. E-mail: dblank@mit.edu

Abbreviations: LTR, localized transport region; PBS, phosphate-buffered saline; RBHE, rhodamine B hexyl ester; SLS, sodium lauryl sulfate; SRB, sulforhodamine B; TPM, two-photon microscopy; US, ultrasound

Received 6 September 2006; revised 6 February 2007; accepted 15 March 2007; published online 7 June 2007

Table 1. Relevant physical properties of the fluorescent *hydrophilic* probe, SRB, and of the fluorescent *hydrophobic* probe, RBHE, examined with two-photon microscopy (Yu *et al.*, 2001)

Probe	Molecular weight (Da)	Absorbance/emission (nm)[1]	Log $K_{O/PBS}$ [2]
SRB	559	565/586	-0.45 ± 0.0045
RBHE	627	556/578	2.49 ± 0.18

rhodamine B hexyl ester, RBHE; sulforhodamine B, SRB.
[1]Fluorescence absorbance and emission wavelengths of SRB and RBHE.
[2]Octanol – phosphate-buffered saline partition coefficient.

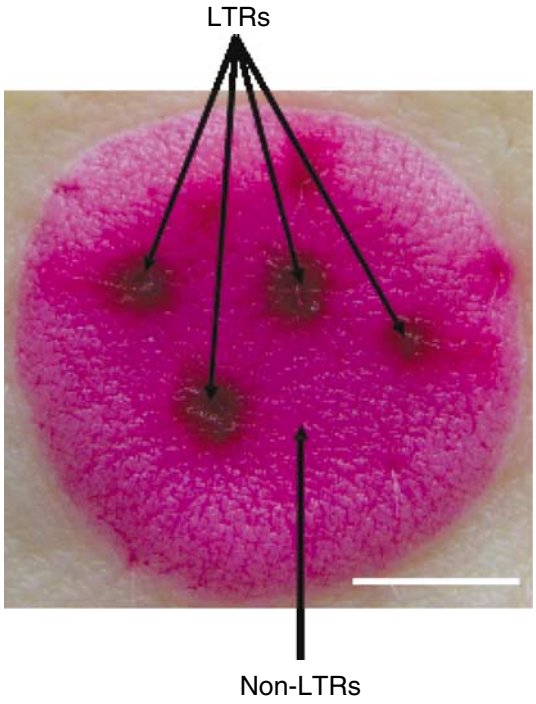

Figure 1. Sample macroscopic image of the LTRs and of the surrounding regions of the skin (the non-LTRs), as indicated by the black arrows. LTRs are formed in skin treated with US in the presence of a red fluorescent permeant (Kushner *et al.*, 2004). Bar = 5 mm.

primary pathways in the stratum corneum of the non-LTRs (see Figure 1) (Kushner *et al.*, 2004). *Dual-channel* TPM is performed in the current investigation to evaluate whether transcellular or intercellular transdermal transport pathways are utilized by SRB and RBHE in the LTRs and in the non-LTRs of skin treated simultaneously with low-frequency US and SLS as well as in the LTRs and in the non-LTRs of US-treated skin, and SLS-treated skin relative to untreated skin (the control) (see Results and Discussion). Dual-channel TPM allows for simultaneous imaging of the exogenous fluorescent permeant (i.e., SRB or RBHE) and the intrinsic skin fluorophores (i.e., collagen, elastin, aromatic amino acids, nicotinamide adenine dinucleotide, porphyrins, and flavin adenine dinucleotide; Na *et al.*, 2000, 2001). This method allows the location of SRB or RBHE to be determined relative to the structure of the skin, making it possible to examine whether SRB or RBHE penetrates the corneocyte domain or remains in the intercellular domain (see Materials and Methods). In addition to evaluating the presence of transcellular and intercellular transdermal pathways in each of the six skin types examined in the current investigation, profiles of the average fluorescence intensity of SRB and RBHE as a function of skin depth are generated from the dual-channel TPM images to identify significant differences in the extent and the depth of the penetration of SRB and RBHE as well as to evaluate enhancement in the values of the vehicle-to-skin partition coefficient (K), the fluorescent intensity gradient (dI/dz), and the effective diffusion path length (L) relative to untreated skin (see Results and Discussion).

RESULTS

Qualitative analysis of the dual-channel TPM images

Figures 2 and 3 show samples of the $120 \times 120\,\mu$m dual-channel TPM images obtained for the delivery of the fluorescent permeants, SRB and RBHE, respectively, in each of the six types of skin samples examined in this study: (1) untreated skin, (2) SLS-treated skin, (3) the non-LTRs of US-treated skin, (4) the LTRs of US-treated skin, (5) the non-LTRs of US/SLS-treated skin, and (6) the LTRs of US/SLS-treated skin. In Figures 2 and 3, the red channel images show the locations of SRB and RBHE in the skin, respectively, and the green channel images show the location of the intrinsic skin fluorophores. The vertical intensity scale bar adjacent to each image ranges from values corresponding to high fluorescence intensities (bright red for SRB and RBHE, and bright green for the skin autofluorescence) to values corresponding to no fluorescence intensities (black for both the exogenous probes and the skin autofluorescence). Sample dual-channel TPM images are presented at $z = 0\,\mu$m (the skin surface), $z = 10\,\mu$m, and $z = 40\,\mu$m to provide qualitative information on how the amount and locations of SRB and RBHE change as a function of skin depth in each of the six skin sample types considered. Where appropriate, the location of a representative corneocyte in the stratum corneum has been indicated with a ''C'', and the visualization of the stratum spinosum (SS) layer of the viable epidermis has been indicated with a ''SS''. Horizontal white scale bars, representing a length of $24\,\mu$m, have been included to aid the reader in approximating dimensions. As a control, untreated skin and US/SLS-treated skin imaged using dual-channel TPM in the absence of SRB or RBHE (a negative control) are presented in Figure 4, showing the expected results of the skin structure in the green channel image, obtained from the intrinsic skin fluorophores, and no corresponding image in the red channel because no exogenous fluorophores were included in the coupling medium for these skin samples.

Average fluorescence intensity profiles of SRB and RBHE

Figures 5 and 6 show the average fluorescence intensity profiles of SRB and RBHE, respectively, obtained from the red channel TPM images. In each figure, the average fluorescence intensity of each permeant is plotted on the y axis and

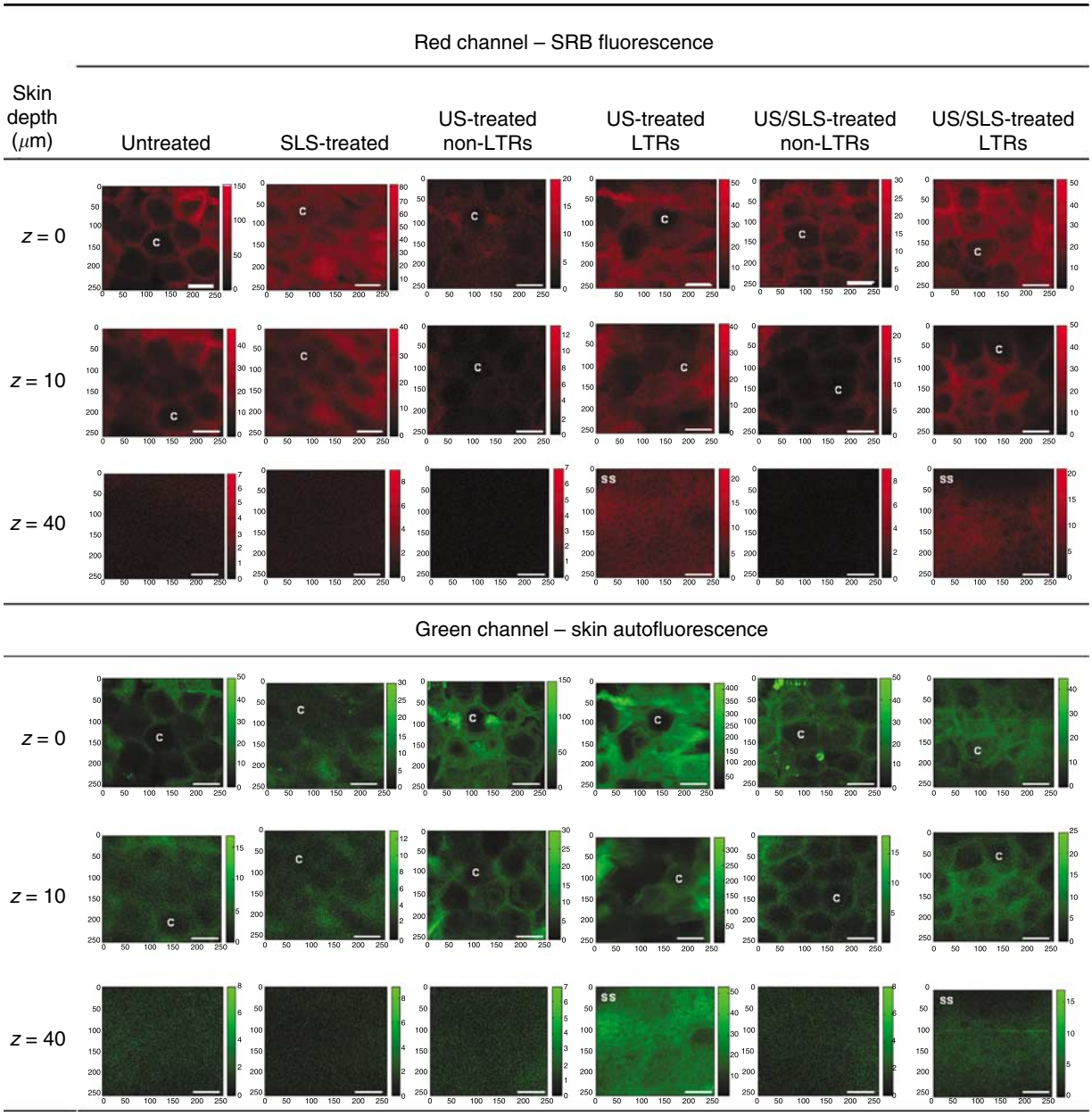

Figure 2. Dual-channel TPM images of SRB in each of the six types of skin samples examined as a function of skin depth (z). C, representative corneocyte; SS, stratum spinosum; horizontal white scale bar, 24 μm. Each image is 120×120 μm. The vertical intensity scale bar adjacent to each image ranges from high fluorescent intensities (bright red for SRB and bright green for the skin autofluorescence) to no fluorescence intensity (black for both the red and the green channels.

the depth (z) from the skin surface (at $z = 0$ μm), in μm, is plotted on the x axis. The error bars represent one standard deviation (SD) in the average value of the permeant fluorescence intensity (for clarity, only the upper error bars are shown in Figures 5 and 6). In addition, the results of the statistical analysis of the fluorescence intensity profiles of each permeant are also shown in Figures 2 and 3. Specifically, a bar (solid or dashed) with a single asterisk (*) indicates the range over which the average fluorescence intensity values from the enhanced skin sample are statistically different ($P<0.05$) from the average fluorescence intensity values from the untreated skin samples. A solid bar with a double asterisk (**) indicates the range over which the average fluorescence intensity values of the LTRs is statistically different ($P<0.05$) from the average fluorescence intensity values of the non-LTRs.

Enhancements in the vehicle-to-skin partition coefficient, the intensity gradient, and the effective diffusion path length for SRB and for RBHE

Tables 2 and 3 report values of the average fluorescence intensity at the skin surface, $I_{(z=0)}$, and of the intensity

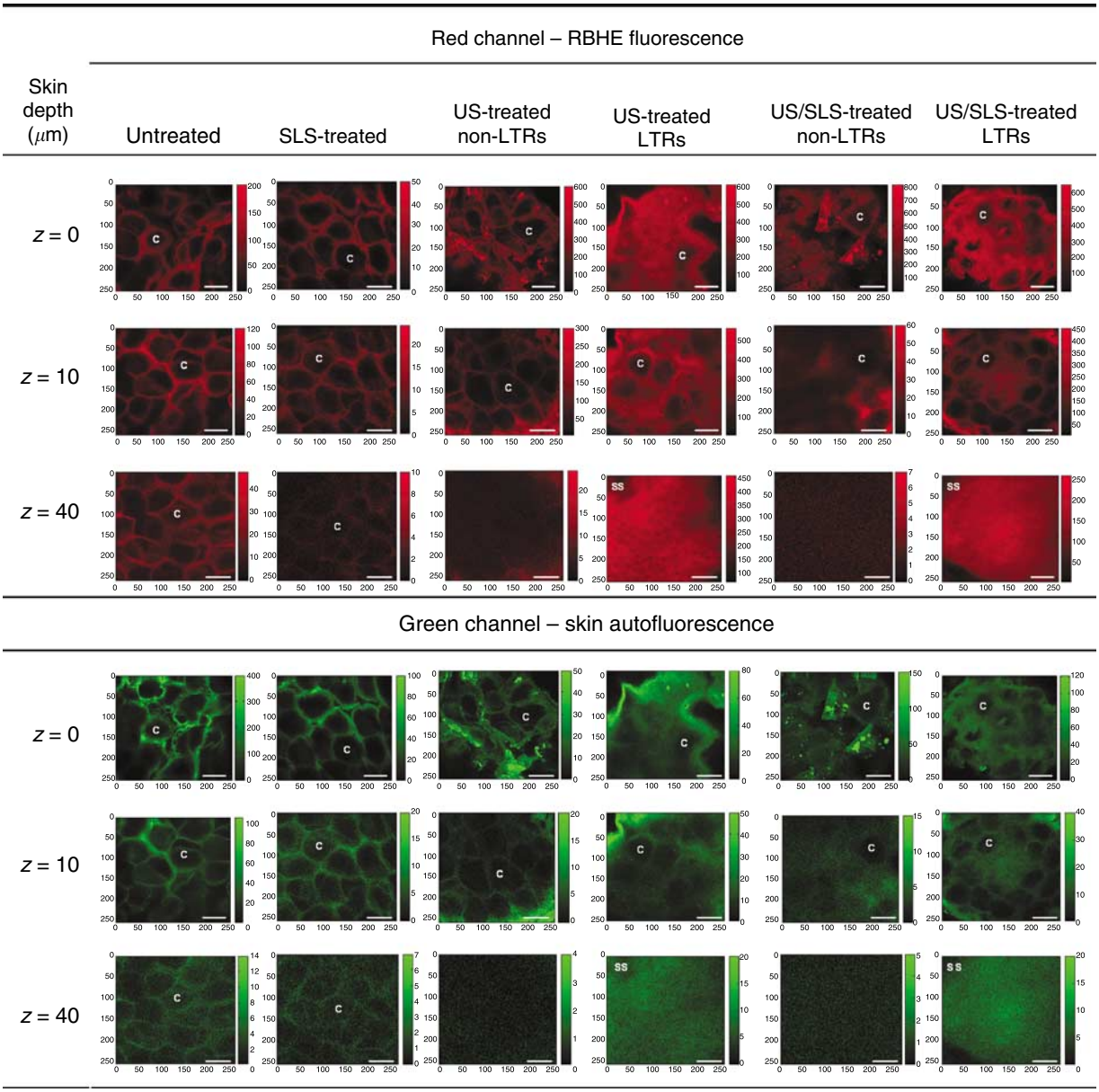

Figure 3. Dual-channel TPM images of RBHE in each of the six types of skin samples examined as a function of skin depth (*z*). C, representative corneocyte; SS, stratum spinosum; horizontal white scale bar, 24 μm. Each image is $120 \times 120\,\mu$m. The vertical intensity scale bar adjacent to each image ranges from high fluorescent intensities (bright red for RBHE and bright green for the skin autofluorescence) to no fluorescence intensity (black for both the red and the green channels.

gradient, d*I*/d*z*, as well as the values of the enhancement in the vehicle-to-skin partition coefficient, E_K, the enhancement in the intensity gradient, E_G, and the enhancement in the effective diffusion path length, E_L, for the delivery of SRB and RBHE, respectively, in each of the five types of enhanced skin samples examined in this study – SLS-treated skin, the non-LTRs and the LTRs of US-treated skin, and the non-LTRs and the LTRs of US/SLS-treated skin. The errors reported for $I_{(z=0)}$, d*I*/d*z*, E_K, E_G, and E_L are presented as ± 1 SD. Values of $I_{(z=0)}$ and d*I*/d*z* corresponding to the enhanced skin samples presented in bold are significantly different ($P<0.05$) from the values of $I_{(z=0)}$ and d*I*/d*z* corresponding to the untreated skin samples.

Investigation of the existence of transcellular permeation pathways in the stratum corneum

Figure 7a and b show a sample plot of the normalized average fluorescence intensity (plotted on the *y* axis) across a five pixelwide slice of the dual-channel TPM image for the delivery of SRB and RBHE, respectively, in the six types of skin samples examined (note that a plot for the delivery of SRB and RBHE in untreated skin was selected for illustrative purposes), as a function of the length of the slice, ranging in value from 0 to 255 pixels (plotted on the *x* axis). The red and the green curves in Figure 7 correspond to the normalized average SRB fluorescence intensity curve and to the normalized average fluorescence intensity curve of the skin

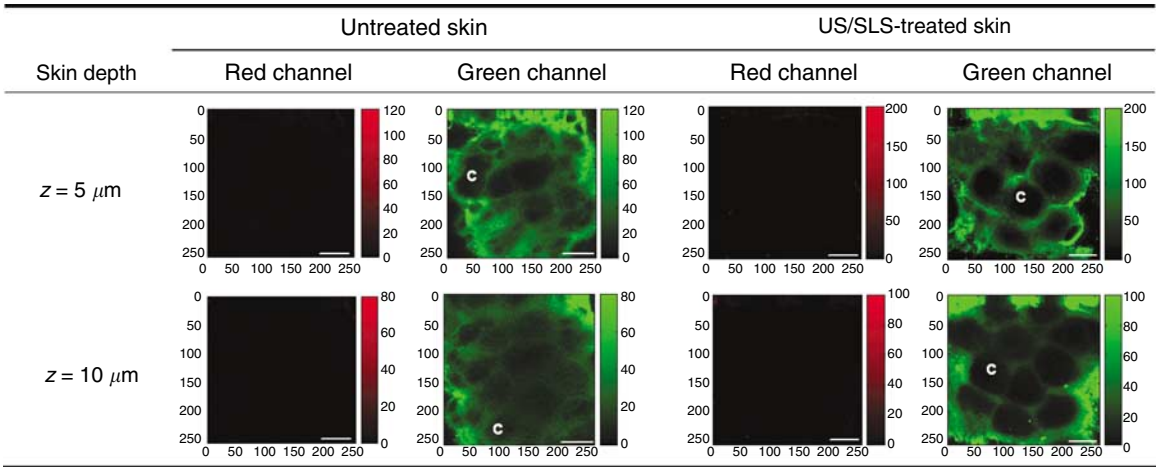

Figure 4. Dual-channel TPM images in the absence of exogenous fluorescent permeant in untreated skin and in US/SLS-treated skin at depths of 5 and 10 μm. C, representative corneocyte; horizontal white scale bar, 24 μm. Each image is 120 × 120 μm. The vertical intensity scale bar adjacent to each image ranges from high fluorescent intensities (bright red for exogenous permeant and bright green for the skin autofluorescence) to no fluorescence intensity (black for both the red and the green channels).

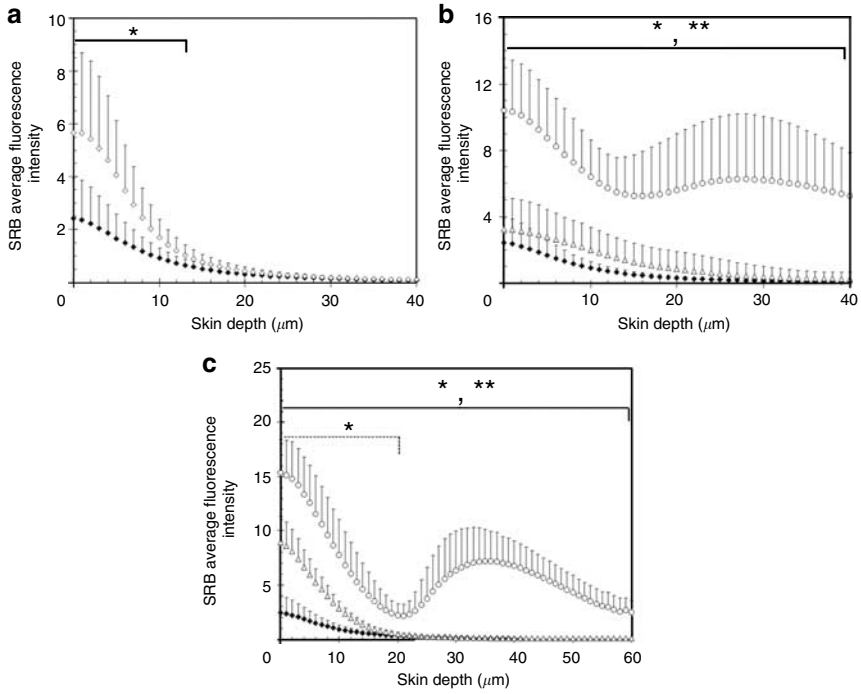

Figure 5. SRB average fluorescence intensity profiles as a function of skin depth (*z*) from the skin surface (at $z = 0\,\mu m$). (**a**) SLS-treated skin versus untreated skin, (**b**) the non-LTRs and the LTRs of US-treated skin versus untreated skin, and (**c**) the non-LTRs and the LTRs of US/SLS-treated skin versus untreated skin. Black diamonds, untreated skin samples; open diamonds, SLS-treated skin samples; open triangles, the non-LTRs; open circles, the LTRs. Error bars represent 1 SD in the average value of 5–7 skin samples. For clarity, only the upper error bars are shown. Single asterisks (*) indicate regions of significant difference ($P<0.05$) between SRB delivery in enhanced skin and in untreated skin. Double asterisks (**) indicate regions of significant difference ($P<0.05$) between SRB delivery in the non-LTRs and in the LTRs. (**c**) The dashed line with the single asterisk (*) corresponds to the confidence interval for the non-LTRs.

autofluorescence, respectively. The various vertical arrows have been included to assist in identifying the peaks in the green curves, which denote the location of the intercellular regions of the stratum corneum. Table 4 reports the measured values of the average heights and of the average widths of the peaks in the red curves at the skin surface ($z = 0\,\mu m$), corresponding to the delivery of SRB (Figure 7a) and of RBHE (Figure 7b), in each of the six types of skin samples examined. Table 5 reports similar values at a depth of $z = 3\,\mu m$ for the skin samples that have significant transcellular penetration at the skin surface ($z = 0\,\mu m$). In Tables 4 and 5, the values are reported as the average measurements, ± 1 SD, of the heights and the widths of 3–5 peaks. Values of peak widths and peak heights shown in bold are significantly

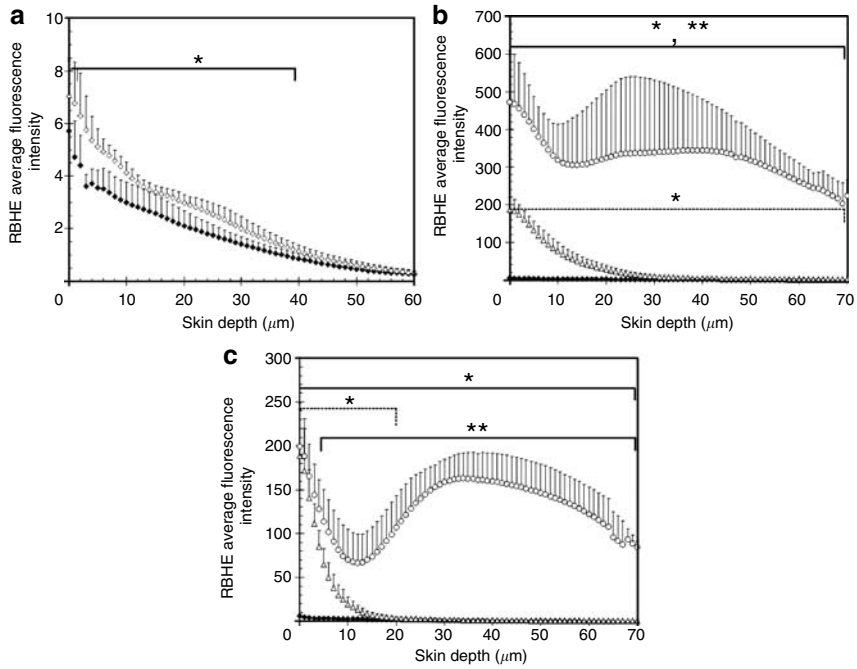

Figure 6. RBHE average fluorescence intensity profiles as a function of skin depth (z) from the skin surface (at $z=0\,\mu$m). (**a**) SLS-treated skin versus untreated skin, (**b**) the non-LTRs and the LTRs of US-treated skin versus untreated skin, and (**c**) the non-LTRs and the LTRs of US/SLS-treated skin versus untreated skin. Black diamonds, untreated skin samples; open diamonds, SLS-treated skin samples; open triangles, the non-LTRs; open circles, the LTRs. Error bars represent 1 SD in the average value of 5–7 skin samples. For clarity, only the upper error bars are shown. Single asterisks (*) indicate regions of significant difference ($P<0.05$) between RBHE delivery in enhanced skin and in untreated skin. Double asterisks (**) indicate regions of significant difference ($P<0.05$) between RBHE delivery in the non-LTRs and in the LTRs. (**b** and **c**) The dashed lines with the single asterisks (*) correspond to the confidence intervals for the non-LTRs.

Table 2. Calculated values of the vehicle-to-skin partition coefficient enhancement, E_K, the intensity gradient enhancement, E_G, and the effective diffusion path length enhancement, E_L, for the delivery of SRB in each of the five types of enhanced skin samples examined obtained from the values of the average fluorescence intensity at the skin surface $I_{(z=0)}$, and of the intensity gradient, dI/dz[1,2,3]

Skin type	$I_{z=0}$	dI/dz	E_K	E_G	E_L
Untreated	2.42±1.52	−0.157±0.004	—	—	—
SLS-treated	**5.67±3.04**	**−0.426±0.020**	2.34±1.93	2.78±0.14	0.84±0.70
US-treated (non-LTRs)	3.28±1.88	**−0.135±0.005**	1.35±1.15	0.86±0.04	1.58±1.25
US-treated (LTRs)	**10.4±3.08**	**−0.439±0.015**	4.32±2.99	2.79±0.12	1.55±1.00
US/SLS-treated (non-LTRs)	**8.92±2.39**	**−0.632±0.012**	3.69±2.51	4.02±0.13	0.92±0.37
US/SLS-treated (LTRs)	**15.4±3.05**	**−0.827±0.037**	6.36±4.18	5.26±0.27	1.21±0.41

LTR, localized transport regions; SLS, sodium lauryl sulfate; SRB, sulforhodamine B; US, ultrasound.
[1]E_K, E_G, and E_L were calculated using equations (1)–(3) (see Materials and Methods).
[2]The errors in $I_{(z=0)}$, dI/dz, E_K, E_G, and E_L are 1 SD.
[3]Values of $I_{(z=0)}$ and dI/dz corresponding to enhanced skin samples presented in bold are significantly different ($P<0.05$) from the values of $I_{(z=0)}$ and dI/dz corresponding to untreated skin samples.

different ($P<0.05$) from the values of peak widths and peak heights corresponding to the delivery of SRB and RBHE in untreated skin.

DISCUSSION

Qualitative analysis of the dual-channel TPM images

On the basis of dual-channel TPM images presented in Figures 2 and 3, three qualitative statements can be made regarding the delivery of SRB and RBHE in the six skin sample types considered. First, *more SRB and RBHE penetrate into the corneocytes at the surface* (see $z=0\,\mu$m for the red channel in Figures 2 and 3) *of the LTRs in both US-treated and US/SLS-treated* skin (both for SRB and RBHE) *as well as for SRB delivery in SLS-treated skin, compared to untreated skin*. This statement is based on the observed uniform distribution of SRB and RBHE between the intercellular and

Table 3. Calculated values of the vehicle-to-skin partition coefficient enhancement, E_K, the intensity gradient enhancement, E_G, and the effective diffusion path length enhancement, E_L, for the delivery of RBHE in each of the five types of enhanced skin samples examined obtained from the values of the average fluorescence intensity at the skin surface $I_{(z=0)}$, and of the intensity gradient, dI/dz[1,2,3]

Skin type	$I_{(z=0)}$	dI/dz	E_K	E_G	E_L
Untreated	5.73±2.74	−0.207±0.034	—	—	—
SLS treated	7.04±1.34	**−0.279±0.018**	1.23±0.63	1.35±0.24	0.91±0.49
US treated (non-LTRs)	**186±33**	**−11.71±0.35**	32.5±16.6	56.6±9.5	0.57±0.31
US treated (LTRs)	**473±136**	**−16.32±0.51**	82.5±46.0	78.8±13.3	1.05±0.61
US/SLS treated (non-LTRs)	**189±52**	**−16.25±1.61**	33.0±18.2	78.5±15.1	0.42±0.25
US/SLS treated (LTRs)	**199±48**	**−12.57±0.95**	34.9±18.7	60.7±11.0	0.57±0.32

LTR, localized transport regions; rhodamine B hexyl ester, RBHE; SLS, sodium lauryl sulfate; US, ultrasound.
[1]E_K, E_G, and E_L were calculated using equations (1)–(3) (see Materials and Methods).
[2]The errors in $I_{(z=0)}$, dI/dz, E_K, E_G, and E_L are 1 SD.
[3]Values of $I_{(z=0)}$ and dI/dz corresponding to enhanced skin samples presented in bold are significantly different ($P<0.05$) from the values of $I_{(z=0)}$ and dI/dz corresponding to untreated skin samples.

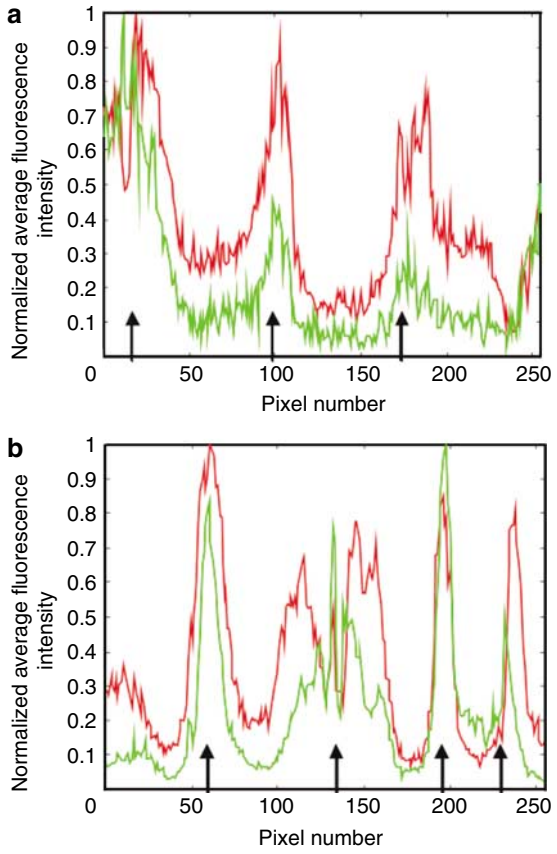

Figure 7. Normalized fluorescent probe and skin autofluorescence intensities in untreated skin. Autofluorescence intensities (*y* axis) are expressed as a function of the pixel number along the length of the image slice (*x* axis). (**a**) SRB and (**b**) RBHE. Red, fluorescent probe; green, skin autofluorescence; vertical arrows, location of intercellular region.

corneocyte domains in the red channel image in the five skin samples identified above relative to untreated skin, where both SRB and RBHE appear to be localized primarily in the intercellular domain. Second, as the depth is increased from $z=0$ to $z=10\,\mu$m, the shapes of the corneocytes in the red channel images of SRB and RBHE become more distinct in the five skin samples identified above, indicating that *less SRB and RBHE penetrate into the corneocytes in the deeper layers of the stratum corneum in the LTRs of US-treated and US/SLS-treated skin as well as for SRB delivery in SLS-treated skin, relative to the penetration into the corneocytes at the surface of these five skin samples.* Third, changes in the structure of the skin in the LTRs of US-treated and US/SLS-treated skin are observed from $z=0$ to $z=10\,\mu$m, where the corneocytes of the stratum corneum (diameter: 30–40 μm) are observed in both the red and the green channels, to $z=40\,\mu$m, where a smaller pattern of dots (diameter: 2–3 μm) is observed in both the red and the green channels. These dots have similar dimensions to the nuclei of cells located in the SS layer of the viable epidermis (Montaga *et al.*, 1992), suggesting that *SRB and RBHE penetrate into the viable epidermis in the LTRs of both US-treated and US/SLS-treated skin.* For the remaining skin samples, there is either no significant SRB and RBHE penetration at $z=40\,\mu$m (see untreated and SLS-treated skin for SRB and the non-LTRs for both US-treated and US/SLS-treated skin for both SRB and RBHE) or the presence of the corneocytes (see untreated and SLS-treated skin for RBHE), suggesting that the penetration of SRB and RBHE is restricted to the stratum corneum.

Analysis of the average fluorescence intensity profiles of SRB

In Figure 5a, the SRB average intensity profile in SLS-enhanced skin (open diamonds) is compared to the SRB average intensity profile in untreated skin (black diamonds). As indicated by the solid bar with a single asterisk (*) in Figure 5a, there is a significant increase ($P<0.05$) in the average intensity of SRB in the first 14 μm of the SLS-treated skin as compared with the average intensity of SRB in the first 14 μm of the untreated skin. In addition, the SRB average fluorescence intensity decreases to near zero values over the first 20 μm of both SLS treated and untreated skin, indicating

Table 4. Measured values of the normalized average peak heights and of the average peak widths[1] for the delivery of SRB and RBHE at the surface ($z = 0\ \mu m$) in each of the six types of skin samples examined[2,3]

	SRB		RBHE	
Skin type	**Height[4]**	**Width[5]**	**Height[4]**	**Width[5]**
Untreated	0.61 ± 0.07	17 ± 3	0.65 ± 0.15	14 ± 5
SLS-treated	**0.46 ± 0.07**	**30 ± 6**	0.82 ± 0.09	**8 ± 1**
US-treated (non-LTRs)	0.79 ± 0.16	16 ± 5	0.68 ± 0.24	25 ± 15
US-treated (LTRs)	**0.25 ± 0.11**	**38 ± 4**	**No discernible peaks**	
US/SLS-treated (non-LTRs)	0.53 ± 0.12	17 ± 5	0.65 ± 0.28	23 ± 11
US/SLS-treated (LTRs)	**0.24 ± 0.05**	**21 ± 5**	0.58 ± 0.14	**30 ± 9**

LTR, localized transport regions; RBHE, rhodamine B hexyl ester; SLS, sodium lauryl sulfate; SRB, sulforhodamine B; US, ultrasound.
[1]The peak width was evaluated at half of the height of the peaks.
[2]The errors are presented as 1 SD in the average.
[3]Values in bold are significantly different ($P < 0.05$) from the values for untreated skin.
[4]The height is presented as a dimensionless quantity, normalized by the maximum value of the fluorescent permeant intensity at $z = 0\ \mu m$.
[5]The width is presented in units of pixels.

Table 5. Measured values of the average peak height and of the average peak width[1] for the delivery of SRB and RBHE at $z = 3\ \mu m$ in skin samples exhibiting significant probe penetration at the skin surface[2,3]

	SRB		RBHE	
Skin type	**Height[4]**	**Width[5]**	**Height[4]**	**Width[5]**
Untreated skin	0.61 ± 0.06	15 ± 2	0.69 ± 0.09	13 ± 5
SLS-treated	**0.36 ± 0.13**	**30 ± 2**	**No entry at $z = 0\ \mu m$**	
US-treated (LTRs)	**0.44 ± 0.09**	**37 ± 5**	**0.27 ± 0.09**	38 ± 25
US/SLS-treated (LTRs)	0.60 ± 0.12	**25 ± 5**	0.45 ± 0.19[6]	24 ± 14

LTR, localized transport regions; RBHE, rhodamine B hexyl ester; SLS, sodium lauryl sulfate; SRB, sulforhodamine B; US, ultrasound.
[1]The peak width was evaluated at half of the height of the peaks.
[2]The errors are presented as 1 SD in the average.
[3]Values in bold are significantly different ($P < 0.05$) from the values for untreated skin.
[4]The height is presented as a dimensionless quantity.
[5]The width is presented in units of pixels.
[6]A statistical difference in the height of the RBHE peaks in the LTRs of US/SLS-treated skin and of untreated skin exists at a level of $P < 0.10$, corresponding to a 90% confidence interval.

that *the stratum corneum (whose thickness is typically of the order of 20 μm* (Schaefer and Redelmeier, 1996)*) provides the primary barrier to the delivery of SRB in SLS-treated skin, similar to untreated skin*. Furthermore, there is little penetration of SRB into the skin deeper than 20 μm in both SLS-treated skin and in untreated skin, confirming that *SRB penetration is confined solely to the stratum corneum in SLS treated and in untreated skin*.

In Figure 5b and c, the SRB average intensity profiles of the non-LTRs (open triangles) and of the LTRs (open circles) in US-treated and in US/SLS-treated skin are compared with the SRB average intensity profile in untreated skin (black diamonds), respectively. The average intensity of SRB within the LTRs of US-treated and of US/SLS-treated skin is significantly greater ($P < 0.05$) than the average intensity of SRB within both untreated skin (as shown by the solid bars with a single asterisk (*)) and the non-LTRs of US-treated and of US/SLS-treated skin (as shown by the solid bars with a double asterisk (**)) over the depth of skin imaged in Figure 5b and c. However, the intensity of SRB in the non-LTRs is only significantly greater ($P < 0.05$) than that of untreated skin in the first 21 μm of US/SLS-treated skin (as shown by the dashed bar with a single asterisk (*) in Figure 5). Furthermore, the average intensity of SRB in the non-LTRs of both US-treated and US/SLS-treated skin decreases rapidly toward near zero intensity in the first 20–30 μm from the skin surface (see Figure 5b and c, respectively). These results confirm that *the extent and the depth of SRB penetration into the LTRs of US-treated and of US/SLS-treated skin are greater than the extent and the depth of SRB penetration in both untreated skin and the non-LTRs of US-treated and of US/SLS-treated skin, whereas significant penetration of SRB in the non-LTRs of US-treated and US/SLS-treated skin is restricted to the stratum corneum*. As no enhancement of the non-LTRs was

observed in US-treated skin, this result suggests that *US only perturbs discrete regions of the skin to enhance the transdermal penetration of model permeants*, which is consistent with previous studies examining the penetration of hydrophilic fluorescent permeants in US-treated skin (Alvarez-Román *et al*., 2003). Finally, although the presence of a chemical enhancer (i.e., SLS) during US treatment is not required for the formation and the enhancement of the LTRs, it is necessary to achieve enhancement of the non-LTRs and to create two significant levels of enhancement in skin treated with US. This result independently confirms the presence of two levels of enhancement, as determined recently using calcein permeability and skin electrical resistivity measurements, in skin treated simultaneously with US and SLS (Kushner *et al*., 2004).

Analysis of the average fluorescence intensity profiles of RBHE

In Figure 6a, the RBHE average intensity profile in SLS-enhanced skin (open diamonds) is compared with the RBHE average intensity profile in untreated skin (black diamonds). There is a significant increase ($P<0.05$) in the average intensity of RBHE in the first 40 μm of SLS-treated skin below the skin surface (at $z=0$ μm) compared with the average intensity of RBHE in the first 40 μm of untreated skin below the skin surface (see the solid bar with a single asterisk (*) in Figure 6a). The RBHE average intensity profiles for the SLS-treated skin and for the untreated skin both decrease toward zero intensity in the region in which the stratum corneum is present. Recall that, for RBHE delivery in untreated and in SLS-treated skin, the stratum corneum was observed down to a depth of 40 μm (see the green channel images for untreated and for SLS-treated skin in Figure 3), indicating the existence of a thicker than normal stratum corneum in these skin samples. Therefore, this result suggests that *RBHE penetration is confined solely to the stratum corneum in both SLS treated and in untreated skin*, similar to the case of SRB delivery in SLS treated and in untreated skin discussed above.

In Figure 6b and c, the RBHE average intensity profiles of the non-LTRs (open triangles) and of the LTRs (open circles) in US-treated and in US/SLS-treated skin are compared, respectively, to the RBHE average intensity profile in untreated skin (black diamonds). In Figure 6b, the average intensity of RBHE in the non-LTRs and in the LTRs of US-treated skin is significantly ($P<0.05$) greater than the average intensity of RBHE in untreated skin, over the entire depth of skin imaged (see the dashed and the solid bars with a single asterisk (*)). In Figure 6c, the average intensity of RBHE in US/SLS-treated skin is significantly ($P<0.05$) greater than the average intensity of RBHE in untreated skin in the first 21 μm for the non-LTRs of US/SLS-treated skin (see the dashed bar with a single asterisk (*)) and over the entire depth of skin imaged for the LTRs of US/SLS-treated skin (see the solid bar with a single asterisk (*)). These results indicate that *more RBHE penetrates into the skin within both the non-LTRs and the LTRs of both US- and US/SLS-treated skin relative to untreated skin*. In addition, the average intensity of RBHE in the non-LTRs of both US-treated and US/SLS-treated skin decreases rapidly toward near zero intensity in the first 20–30 μm, the region where the stratum corneum is located, whereas the average intensity of RBHE in the LTRs of both US-treated and US/SLS-treated skin maintains a high value at depths greater than 30 μm. This result suggests that *RBHE penetration into the non-LTRs of US/SLS-treated skin is confined solely to the stratum corneum, while RBHE penetration into the LTRs of both US-treated and US/SLS-treated skin extends into the viable epidermis.* Finally, because the intensity of RBHE in the LTRs is significantly ($P<0.05$) greater than the intensity of RBHE in the non-LTRs over the entire depth of US-treated skin imaged and at depths greater than 4 μm in US/SLS-treated skin (see the solid bar with a double asterisk (**) in Figures 3c and 6b, respectively), one may conclude that *two levels of skin perturbation also take place for the delivery of RBHE in both US-treated and US/SLS-treated skin,* similar to the case of SRB delivery in US/SLS-treated skin.

Effect of changes in the skin morphology and barrier properties on the shape of the probe average fluorescence intensity profiles within the LTRs of US-treated and of US/SLS-treated skin

In Figures 5b, 5c, 6b, and 6c, after an initial linear decrease of the average fluorescence intensity profiles in the LTRs in the region of the skin corresponding to the stratum corneum ($z=0$ to $z=15$–20 μm), the average fluorescence intensity increases as the skin depth (z) increases in the upper layers of the viable epidermis. Because the average fluorescence intensity is proportional to the total amount of SRB or RBHE present in each layer of the skin, the observed increase in the average fluorescence intensity profiles in the LTRs in the upper layers of the viable epidermis indicates that the *total amount of SRB or RBHE in each layer increases* as a function of skin depth over this range. According to the principles of diffusive transport, the *concentration of SRB or RBHE in each layer must decrease* as a function of depth in the upper layers of the viable epidermis to maintain the flux of SRB or RBHE through the skin. The concentration of SRB or RBHE in each imaged skin layer is defined as the total amount of SRB or RBHE divided by the volume of the imaged skin layer available to SRB or RBHE transport. Since concentration must decrease and the average fluorescence intensity profiles in the LTRs are observed to increase in the upper layers of the viable epidermis, the volume of the imaged skin layer available to transport must increase by more than the total amount of SRB or RBHE increases over the same range. Since the thickness of the focal plane does not increase with imaging depth, only the cross-sectional area of the imaged layer of skin available to transport can increase in the upper layers of the epidermis.

The upper layers of the viable epidermis comprise the stratum granulosum, which serves as a transitional layer between the stratum corneum and the SS of the viable epidermis (Schaefer and Redelmeier, 1996). As one moves from the stratum corneum through the stratum granulosum to the SS, the diameter of the skin cells gradually decreases from a diameter of 40 μm in the stratum corneum (Johnson *et al*., 1997) to a diameter of 10–12 μm in the viable epidermis

(Schaefer and Redelmeier, 1996), which results in a gradual increase in the fraction of the skin occupied by the intercellular domain from 8–9% in the stratum corneum (Johnson *et al.*, 1997) to 15% in the viable epidermis (Schaefer and Redelmeier, 1996). In addition, the barrier properties of the skin cells decrease as one moves from the stratum corneum through the stratum granulosum to the SS. The formation of the cornified envelope, a highly cross-linked network of covalently bound proteins and lipids that surrounds the corneocytes of the stratum corneum and is responsible for providing the cell membrane resistance to permeant transport, begins in the upper layers of the SS and continues to develop in the stratum granulosum (Schaefer and Redelmeier, 1996). Therefore, as one moves from the stratum corneum through the stratum granulosum to the SS, SRB and RBHE can more easily penetrate inside the skin cells (compare the red channel images at $z = 10\ \mu$m and $z = 40\ \mu$m for the LTRs in both US-treated and US/SLS-treated skin in Figures 2 and 3). Both of these effects – decreased cell diameter and reduced barrier properties – lead to an increase in the cross-sectional area available to transport as a function of skin depth in the stratum granulosum.

It is noteworthy that the shapes of the average fluorescence intensity profiles in the LTRs are not dependent on the presence of SLS during US treatment or on the physicochemical properties of SRB and RBHE. It should also be noted that the increase in the average intensity of SRB and RBHE in the upper layers of the viable epidermis is less pronounced in Figures 5b and 6b than in Figures 5c and 6c. Recall that for the case of US treatment, the skin is exposed to SRB and RBHE for 24 hours before imaging, whereas for the case of US/SLS treatment, the skin is exposed to SRB and RBHE for only 5–10 minutes before imaging (see Materials and Methods). Therefore, for the US-treated skin experiments, SRB and RBHE have more time to fully penetrate into the lower layers of the stratum corneum (compare the red channel images for $z = 10\ \mu$m in the LTRs of US-treated skin with the LTRs of US/SLS-treated skin in Figures 2 and 3) and in the upper layers of the viable epidermis, allowing for a more uniform distribution of SRB and RBHE in these skin layers as a function of skin depth.

Analysis of the enhancements in the vehicle-to-skin partition coefficient, the intensity gradient, and the effective diffusion path length for SRB and for RBHE

A significant increase ($P < 0.05$) in the magnitudes of $I_{(z=0)}$ and dI/dz relative to untreated skin are observed in SLS-treated skin, the LTRs of US-treated skin, and the non-LTRs and the LTRs of US/SLS-treated skin for the delivery of SRB (see Table 2), and in both, the non-LTRs and the LTRs of US-treated and US/SLS-treated skin, for the delivery of RBHE (see Table 3). The corresponding values for E_K and E_G in these skin samples are all much larger than unity (see Tables 2 and 3), although this trend is not observed for the values of E_L calculated using equation (3) (see Materials and Methods), suggesting that there is no significant alteration of the effective diffusion path used by SRB and RBHE in these skin samples. Also, because the values of E_L are small compared to the values of E_G, the observed enhancement in the intensity gradient in these skin samples is primarily due to an enhancement in the value of $I_{(z=0)}$ from SLS and/or US treatment of the skin. However, for the delivery of SRB in the non-LTRs of US-treated skin, because there is only a small significant decrease ($P < 0.05$) in the magnitude of dI/dz and no significant difference in the value of $I_{(z=0)}$ relative to untreated skin, the corresponding values of E_K, E_G, and E_L are not very different from unity, suggesting that *delivery of SRB in the non-LTRs of US-treated skin is similar to the delivery of SRB in untreated skin*. Similarly, for the delivery of RBHE in SLS-treated skin, because there is only a small significant increase ($P < 0.05$) in the magnitude of dI/dz and no significant difference in the value of $I_{(z=0)}$ relative to untreated skin, the corresponding values of E_K, E_G, and E_L are once again not very different from unity, suggesting that the *delivery of RBHE in SLS-treated skin is similar to the delivery of RBHE in untreated skin*. Finally, for the delivery of SRB, the values of $I_{(z=0)}$ and dI/dz corresponding to the non-LTRs in US/SLS-treated skin are both significantly different ($P < 0.05$) than the values of $I_{(z=0)}$ and dI/dz corresponding to the LTRs in US/SLS-treated skin, further confirming *the existence of two levels of perturbation in skin treated simultaneously with US and the chemical enhancer, SLS*. However, for the delivery of RBHE, the values of both $I_{(z=0)}$ and dI/dz are significantly different ($P > 0.05$) for the LTRs relative to the non-LTRs in both US-treated and US/SLS-treated skin. This result further confirms that, contrary to the case of SRB delivery, *two levels of skin perturbation are present in both US-treated and US/SLS-treated skin for the delivery of RBHE*.

Impact of ethanol, a chemical enhancer, on the delivery of RBHE

From a comparison of the results for the delivery of SRB and RBHE reported in the previous sections, there are two cases where the results for SRB and RBHE differ: (i) SLS-treated skin relative to untreated skin and (ii) the non-LTRs of US-treated skin relative to untreated skin. The observed differences can be attributed to the presence of ethanol in the RBHE donor solution, which was required to solubilize RBHE, a hydrophobic permeant, in phosphate-buffered saline (PBS) (see Materials and Methods). Ethanol, however, can serve as a chemical enhancer for the transdermal delivery of both hydrophobic permeants (Femenia-Fonta *et al.*, 2005; Johnson *et al.*, 1996; Bhatia *et al.*, 1997; Magnusson and Runn, 1999; Pillai *et al.*, 2004) and hydrophilic permeants (Peck *et al.*, 1994). Noting that ethanol was present at a concentration of 50% (v/v), whereas SLS was present only at a concentration of 1% (w/v), the enhancing effect of SLS on the transdermal delivery of RBHE is expected to be small relative to that of ethanol. Indeed, there was only a 23% increase in the surface concentration of RBHE and a 35% increase in the intensity gradient of RBHE after a 24 hours treatment with 1% SLS relative to untreated skin. This result is similar to the 70–140% enhancement in the permeability of mannitol in 50:50 mixture of ethanol and PBS after a 40 hours treatment with 1% SLS (Karande and Mitragotri, 2002) relative to

untreated skin. Furthermore, the presence of ethanol in the RBHE coupling medium during US treatment can also explain the increased penetration of RBHE into the non-LTRs of US-treated skin relative to untreated skin, similar to the observation for the delivery of SRB in skin treated simultaneously with US and with a chemical enhancer, SLS. *Therefore, ethanol also acts as a chemical enhancer to create two levels of perturbation for the case of RBHE delivery in US-treated skin.*

Analysis of transcellular permeation pathways in the stratum corneum

For the delivery of SRB in SLS-treated skin, the penetration of SRB into the corneocytes located at $z = 0\,\mu$m in these skin samples *increases* relative to untreated skin, because the average widths of the SRB peaks are significantly larger ($P < 0.05$) and the average heights of the SRB peaks are significantly smaller ($P < 0.05$) than the corresponding fluorescence peaks for untreated skin reported in Table 4. However, for the delivery of RBHE in SLS-treated skin, the penetration of RBHE into the corneocytes located at the surface of SLS-treated skin *decreases* relative to untreated skin, because the average widths of the RBHE fluorescence peaks in SLS-treated skin are significantly smaller ($P < 0.05$) and the average heights of the RBHE fluorescence peaks are approximately 20% larger than the corresponding RBHE peaks in untreated skin reported in Table 4. These results suggest that *SLS increases the partitioning of SRB, a hydrophilic permeant, into the corneocyte domain (a hydrophilic environment) while it localizes RBHE within the intercellular lipid domain of the stratum corneum (a hydrophobic environment).* These findings are consistent with previous studies on the role of the chemical enhancer, oleic acid, on the transdermal delivery of SRB and RBHE (Yu *et al.*, 2003b).

For the delivery of SRB and RBHE in the non-LTRs of US-treated skin and of US/SLS-treated skin, there is no significant difference ($P > 0.05$) in the heights and the widths of the fluorescence peaks when compared to the heights and the widths of the SRB fluorescence peaks in untreated skin (see Table 4). This data provides further evidence that *the delivery of SRB and RBHE in the non-LTRs in both US-treated and US/SLS-treated skin occurs primarily via the intercellular route*, similar to what occurs in untreated skin. For the case of RBHE delivery in the LTRs of US-treated skin, there are no discernable peaks present (data not shown), due to the uniform distribution of RBHE in the corneocytes and in the intercellular regions. Therefore, no peak widths or peak heights are reported in Table 4. For the delivery of SRB in SLS-treated skin and in the LTRs of US-treated skin and of US/SLS-treated skin, and for the delivery of RBHE in the LTRs of US/SLS-treated skin, the penetration of SRB and RBHE into the corneocytes located at $z = 0\,\mu$m in these skin samples *increases* relative to untreated skin, because the average widths of the fluorescence peaks are significantly larger ($P < 0.05$) and the average heights of the fluorescence peaks are significantly smaller ($P < 0.05$) than the corresponding fluorescence peaks for untreated skin reported in Table 4. Furthermore, increased penetration of both SRB and RBHE into the corneocytes of the LTRs of US-treated and US/SLS-treated skin, as well as of SRB into the corneocytes of SLS-treated skin, is also observed at a depth of $z = 3\,\mu$m relative to untreated skin (see Table 5). Using the penetration of SRB and RBHE into the corneocytes at $z = 0\,\mu$m and $z = 3\,\mu$m as a marker for the existence of transcellular permeation pathways in the stratum corneum, these results suggest that *transcellular permeation pathways are utilized in the delivery of SRB and RBHE in the LTRs in both US-treated and US/SLS-treated skin as well as in the delivery of SRB in SLS-treated skin.* This observation independently confirms that transcellular pathways are utilized by hydrophilic (and hydrophobic) permeants in the LTRs of US/SLS-treated skin, as proposed recently based on a macroscopic analysis of the skin electrical resistivity data in the context of the aqueous-pore pathway hypothesis (Kushner *et al.*, 2004).

Proposed mechanisms of enhancement in SLS-, US-, and US/SLS-treated skin

As shown in the previous section, SLS increased the partitioning of SRB into the corneocyte domain and increased the localization of RBHE into the intercellular domain. To achieve these observed results, SLS could either increase the hydrophilicity of the corneocyte domain or increase the hydrophobicity of the intercellular domain. There is ample evidence that SLS increases the hydration (i.e., water uptake) of the stratum corneum (Miyazawa *et al.*, 1984; Rhein *et al.*, 1986; Wilhelm *et al.*, 1993; Goffin *et al.*, 1999; Mizushima *et al.*, 2000), as well as some recent evidence that these hydration effects are localized primarily in the corneocyte domain (Bouwstra *et al.*, 2003; Uhoda *et al.*, 2005; Xhauflaire-Uhoda *et al.*, 2006). Therefore, SLS-induced absorption of water in the corneocytes, which would increase the hydrophilicity of the corneocyte domain, is a possible mechanism for the observed results for the delivery of SRB and RBHE in SLS-treated skin relative to untreated skin.

From previous studies of US-enhanced transdermal drug delivery, it has been demonstrated that transient acoustic cavitation events near the skin surface are the primary mechanism responsible for the observed enhancement of transdermal transport (Tang *et al.*, 2002b; Tezel *et al.*, 2002b; Tezel and Mitragotri, 2003). In the present investigation, SRB delivery was enhanced only in discrete regions of US-treated skin (i.e., the highly permeable LTRs; Kushner *et al.*, 2004) relative to SRB delivery in untreated skin, similar to calcein delivery in US-treated skin (Alvarez-Román *et al.*, 2003). This result suggests that the transient acoustic cavitation events form during US treatment occur in discrete regions, rather than homogeneously, in the acoustic coupling medium near the skin surface. When a transient cavitation bubble implodes near the skin surface, high-velocity microjets are formed and directed toward the surface of the skin (Tang *et al.*, 2002b). Because the corneocytes represent over 99% of the skin surface, it is highly probable that these high-velocity microjets deliver the probe-containing coupling medium into the corneocytes near the skin surface forming the observed

transcellular pathways in the LTRs and facilitating delivery of the probe into the viable epidermis.

When a chemical enhancer (i.e., ethanol or SLS) is present in the coupling medium during US treatment, the delivery of SRB and RBHE in the non-LTRs also increases relative to the delivery of SRB and RBHE in untreated skin. Because the penetration of SRB and RBHE within the non-LTRs did not extend into the corneocytes or the viable epidermis as it did within the LTRs, it is likely that the chemical enhancer is not inducing transient acoustic caviation events in the coupling medium above the surface of the non-LTRs during US treatment. Rather, *acoustic streaming in the coupling medium*, another effect of US treatment of the skin (Wells, 1977), provides additional convective driving forces, which may enhance the delivery and the dispersion of the chemical enhancer (Mitragotri *et al.*, 2000) into the non-LTRs. Once the chemical enhancer penetrates into the skin, it may enhance the transdermal delivery of SRB and RBHE by (i) disordering the intercellular lipid bilayers (Fartasch *et al.*, 1998), (ii) disrupting the corneocyte cornified envelope (Welzel *et al.*, 1998), (iii) extracting lipids from the stratum corneum (Elias, 1996; Alvarez-Román *et al.*, 2003), or (iv) expanding and increasing the connectivity of the lacunar domains present in the intercellular regions of the stratum corneum (Paliwal *et al.*, 2006).

MATERIALS AND METHODS

Chemicals

Phosphate-buffered saline (PBS; 0.01 M phosphate, 0.137 M NaCl) was obtained from Fluka Chemical (St Louis, MO). SRB, a hydrophilic fluorescent probe, and RBHE, a hydrophobic fluorescent probe were obtained from Molecular Probes (Eugene, OR). Ethanol and SLS were obtained from Sigma Chemical Company (St Louis, MO). All these chemicals were used as received.

Skin preparation

All experimental protocols with human tissue were approved by the Committee on the Use of Human Experimental Subjects (COUHES) at MIT and were deemed to be in accordance with the guidelines published in the Declaration of Helsinki Principles. Human full-thickness skin samples from the abdominal area were obtained from the National Disease Research Institute (Philadelphia, PA) and stored at −80°C for up to 3 months before use. Before its use in the fluorescent permeant diffusion experiments (see below), the skin was thawed and the subcutaneous fat was removed from the skin using a razor blade. The skin was then sectioned and mounted in vertical Franz diffusion cells (15-mm inner diameter) obtained from Permegear (Bethlehem, PA). Finally, the initial electrical resistivity of the skin was measured using previously published methods (Tang *et al.*, 2002a). Any skin sample with an initial resistivity lower than 50 kΩ/cm^2, which is indicative of the skin sample being compromised (Tang *et al.*, 2002a), was discarded and replaced with a new skin sample.

Preparation of the fluorescent permeant solutions

For the visualization of SRB in human skin, the following solutions were prepared: Formulation (S-1), 0.05 mg/ml of SRB in PBS; Formulation (S-2), 0.005 mg/ml of SRB in PBS; Formulation (S-3), 0.005 mg/ml of SRB in PBS containing 1% (w/v) SLS. For the visualization of RBHE in human skin, the following solutions were prepared: Formulation (R-1), 0.05 mg/ml of RBHE in a 50/50 mixture of PBS and ethanol; Formulation (R-2), 0.005 mg/ml of RBHE in a 50/50 mixture of PBS and ethanol; Formulation (R-3), 0.005 mg/ml of SRB in a 50/50 mixture of PBS and ethanol containing 1% (w/v) SLS. The concentrations of SRB and RBHE in formulations S-1 to S-3 and R-1 to R-3 were selected for the following reasons. For the enhanced delivery of SRB and RBHE in the skin, a smaller concentration of 0.005 mg/ml was chosen to enable the detection of both the fluorescent permeant and the intrinsic skin autofluorescence signals (Yu *et al.*, 2003b). For the delivery of SRB and RBHE in untreated skin, a larger concentration of 0.05 mg/ml was chosen to ensure that enough fluorescent permeant was present in the skin to be detected with TPM. Ethanol was included in the RBHE solution to enable solubility of RBHE, which is immiscible in PBS due to its relatively high level of hydrophobicity (see Table 1). Finally, 1% (w/v) SLS was selected as the amount of chemical enhancer to be consistent with previous studies on LTRs using low-frequency sonophoresis (Kushner *et al.*, 2004).

Diffusion experiments using fluorescent permeants

Skin samples were divided into four groups: (1) untreated, (2) SLS-treated (chemical enhancer only), (3) US-treated (low-frequency sonophoresis only), and (4) US/SLS-treated (simultaneous application of low-frequency US and a chemical enhancer). For the delivery of SRB and RBHE in untreated skin samples, the skin was exposed to Formulation (S-1) and to Formulation (R-1), respectively, for 24 hours. For the delivery of SRB and RBHE in chemically enhanced skin samples, the skin was exposed to Formulation (S-3) and to Formulation (R-3), respectively, for 24 hours. For the delivery of SRB and RBHE in US-treated skin samples, the skin was exposed to Formulation (S-2) and to Formulation (R-2), respectively, for 24 hours in the presence of US at the following conditions: frequency, 20 kHz; intensity, 1.6 W/cm^2; duty cycle, 0.1:0.9 seconds (ON:OFF); tip displacement, 3 mm. At the end of the 24-hour exposure period, the skin electrical resistivity was measured to determine the extent to which each delivery method had perturbed the structure of the skin. For the delivery of SRB and RBHE in skin samples treated simultaneously with low-frequency US and a chemical enhancer (SLS), the skin was exposed to Formulation (S-3) and to Formulation (R-3), respectively, in the presence of US at the following conditions: frequency, 20 kHz; intensity, 7.5 W/cm^2; duty cycle, 5:5 seconds (ON:OFF); tip displacement, 3 mm, until the skin electrical current reached a value of 225 μA, similar to the conditions examined previously for the study of LTR formation in skin treated simultaneously with low-frequency US and a chemical enhancer (Kushner *et al.*, 2004). Note that this level of skin electrical current was obtained after treating the skin simultaneously with US and SLS for 5–10 minutes.

Preparation of skin samples for TPM imaging

After delivery of SRB and RBHE into the skin, the skin samples were removed from the Franz diffusion cells, and excess formulation was removed from the skin surface by gently blotting the skin surface with a Kimwipe (Kimberly-Clark Corporation, Roswell, GA). The circular region of the skin exposed to the fluorescent permeants was removed using a razor blade. A few drops of PBS were then added to an imaging chamber (2.5 mm Coverwell; Grace Bio Labs, Bend, OR)

covered with a No. 1, 22 mm × 22 mm glass coverslip (VWR Scientific, Media, PA) to ensure good contact of the skin surface with the coverslip. The skin was then inserted into the imaging chamber and subsequently mounted onto a glass microscope slide (VWR Microslides, 25 × 75 mm).

Dual-channel TPM imaging and data collection

Dual-channel TPM imaging of the skin samples was conducted according to previously published methods (Yu *et al.*, 2003b), which are briefly summarized here. The laser source was provided by a femtosecond ti-sa laser (Tsunami, Spectra-Physics, Mountain View, CA) pumped by a 5W diode-pumped, solid state CW laser (Millenia V, Spectra-Physics, Mountain View, CA). For all the dual-channel TPM imaging, the laser power was set at 250 mW to ensure detection of the skin autofluorescence signal, while minimizing damage to the skin from the laser. A modified inverted microscope (Axiovert, 100TV, Ziess, Thornwood, NY) with an oil immersion ×40 objective lens (Zeiss F Fluar, NA.13) was used to image the skin samples. X–Y scans were made with a scanner unit (6350 Cambridge Technology, Watertown, MA). The emitted photons from the laser excitation are collected by the microscope and then passed through two filters, which split the signal into the *red channel* for the photons emitted by the fluorescent permeant and the *green channel* for the photons emitted by the intrinsic skin fluorophores. Splitting of the signal into two channels is possible due to the differences in the fluorescence emission wavelength of the intrinsic skin fluorophores (450 and 520 nm) (Na *et al.*, 2000) and the emission wavelengths of SRB and RBHE (see Table 1). The signals from the red and the green channels are then sent to a photomultiplier and are discriminated against dark noise with a custom-built high-speed photon discriminator to obtain the final dual-channel TPM image. In untreated and in SLS-treated skin, six 120 × 120 μm skin sites were imaged. In US-treated and in US/SLS-treated skin, 12 120 × 120 μm skin sites were imaged – six sites for the non-LTRs and six sites for the LTRs. The depth of the TPM imaging varied from a depth of 40 μm, for skin samples where little to no fluorescent permeant penetrated deep into the skin, to a depth of 70 μm, for skin samples where significant fluorescent permeant penetrated deep into the skin.

Analysis of the TPM images

The techniques that were used to analyze the dual-channel TPM images of both SRB and RBHE are based on previously published methods (Yu *et al.*, 2001, 2003b), which are described briefly in this section. These techniques include: (1) generating and analyzing the average fluorescence intensity profiles for each permeant as a function of skin depth, (2) evaluating the enhancement of the fluorescent permeant vehicle-to-skin partition coefficient, (3) evaluating the enhancement of the fluorescent permeant intensity gradient, (4) evaluating the enhancement of the effective diffusion path length, and (5) evaluating the existence of transcellular permeation pathways in the stratum corneum. All the TPM image processing reported in this section was carried out using MATLAB with the Image Processing Toolbox (Version 7.0.4.365 (R14) Service Pack 2, The Mathworks Inc., Natick, MA).

The average fluorescent permeant intensity profiles as a function of skin depth were generated using an in-lab subroutine in MATLAB, which calculated an average value for the fluorescence intensity, I, (obtained from photons collected during a time of 0.1 ms) for each layer of the skin imaged in the z-direction (the direction perpendicular to the skin surface). The surface of each skin sample, corresponding to $z = 0\,\mu$m, was defined at the location of the first local maximum in the average value of the intensity of the fluorescent probes as a function of increasing skin depth (Yu *et al.*, 2001). The average value of the fluorescence intensity at $z = 0\,\mu$m was then averaged over the 5–7 skin sites imaged for each of the six types of skin samples examined in this study for the delivery of SRB and RBHE: (1) untreated skin, (2) SLS-treated skin, (3) the non-LTRs of US-treated skin, (4) the LTRs of US-treated skin, (5) the non-LTRs of US/SLS-treated skin, and (6) the LTRs of US/SLS-treated skin. For the average fluorescence intensity profiles of SRB and RBHE in untreated skin, the value of I was divided by 10 to account for the difference in the donor concentration of the fluorescent permeant used for the untreated skin samples (0.05 mg/ml) and for the enhanced skin samples (0.005 mg/ml). To determine whether treatment of the skin with SLS, US, or US/SLS results in a significant enhancement in the skin penetration of SRB and RBHE, the average value of the fluorescent permeant intensity in the enhanced skin samples and in the untreated skin samples were analyzed with the t-statistic (Montgomery *et al.*, 1998), which tests for the difference in two average values where the variances are not equal, over the depth of skin imaged. A value of $P = 0.05$, corresponding to a 95% confidence interval, was selected for the analysis of the average fluorescent permeant intensity profiles in this study.

The values for E_K, E_G, and E_L, the enhancement in the vehicle-to-skin partition coefficient, the intensity gradient, and the effective diffusion path length, respectively, were obtained using previously published methods (Yu *et al.*, 2001), which are summarized briefly here (Yu *et al.*, 2001). By assuming that the intensity of the fluorescent permeant, I, is directly proportional to its concentration in the skin, E_K can be approximated from the average fluorescence intensity profiles using the following equation (Yu *et al.*, 2001):

$$E_K = \frac{I_{Enhancer}(z=0)}{I_{Untreated}(z=0)} \quad (1)$$

where $I_{Enhancer}(z=0)$ is the average value of the fluorescence intensity of SRB or of RBHE at the surface of the enhanced skin samples (i.e., SLS-, US-, or US/SLS-treated skin samples) and $I_{Untreated}(z=0)$ is the average value of the fluorescence intensity of SRB or of RBHE at the surface of the untreated skin samples. The fluorescent permeant intensity gradient, (dI/dz), in the stratum corneum was evaluated by performing linear regression using the average intensity values from the first 12 scans from the surface into the stratum corneum, a region which exhibits a significant decrease in the average fluorescent probe intensity in the untreated skin, to which the average fluorescent probe intensities in the enhanced skin samples are then compared (Yu *et al.*, 2001). To calculate the enhancement in the fluorescent permeant intensity gradient, E_G, the following equation was used (Yu *et al.*, 2001):

$$E_G = \frac{(dI/dz)_{Enhanced}}{(dI/dz)_{Untreated}} \quad (2)$$

where $(dI/dz)_{Enhanced}$ and $(dI/dz)_{Untreated}$ are the fluorescent permeant intensity gradients corresponding to the intensity profiles of the enhanced skin samples and of the untreated skin samples, respectively. The enhancement in the effective diffusion path length, E_L, in enhanced skin samples as compared to untreated skin samples

can then be evaluated from the values of E_K and E_G as follows (Yu *et al.*, 2001):

$$E_L = \frac{E_K}{E_G} \quad (3)$$

The identification of transcellular pathways from an analysis of the dual-channel TPM images is based on previously published methods (Yu *et al.*, 2003b). A slice, 5 pixels (width) × 256 pixels (length), of the red channel (probe) and of the green channel (skin autofluorescence) TPM images was selected for analysis of the location of the fluorescent permeant relative to the structure of the skin. At each position along the length of this slice (0–255 pixels), the intensities of the corresponding five pixels along the width were averaged and then normalized. These normalized average values, for both the red channel and the green channel, were plotted as a function of the pixel number along the length of the slice. Previous studies utilizing this dual-channel TPM image analysis technique have demonstrated that it is possible to determine whether there is an increase, or a decrease, in the penetration of the fluorescent probe into the corneocytes (Yu *et al.*, 2003b). Specifically, by measuring the widths and the heights of peaks in the normalized average intensity profile of the fluorescent probe in untreated skin, and subsequently comparing these values to the peak widths and the peak heights of the fluorescent probe in the enhanced skin samples, enhancements, or reductions, in the penetration of the fluorescent probe into the corneocytes can be evaluated quantitatively. As the heights of the peaks increase and as the widths of the peaks decrease, there is less fluorescent permeant present inside the corneocytes, which serves as a qualitative indicator of the existence of *intercellular permeation pathways*. Conversely, as the heights of the peaks decrease and as the widths of the peaks increase, there is more fluorescent permeant present inside the corneocytes, which serves as a qualitative indicator of the existence of *transcellular permeation pathways*. The height of a peak was determined by evaluating the difference between the height of the peak and the average height of the two valleys that neighbor the peak. The width of a peak was determined by measuring the width of the peaks at half of the peak height. The skin surface ($z = 0\,\mu$m) was selected as the skin layer to identify the entries into the transcellular permeation pathways. The surface of the skin is the first skin layer that is perturbed by SLS or by US, because it is at the skin surface where the enhancing transient acoustic cavitation events occur (Tang *et al.*, 2002a, b; Tezel *et al.*, 2002a, b; Tezel and Mitragotri, 2003), and where the skin contacts the coupling medium. For samples with transcellular pathway entries present at $z = 0\,\mu$m, additional measurements of the peak heights and the peak widths were made at $z = 3\,\mu$m to demonstrate that the transcellular pathways do indeed extend into the stratum corneum. Note that this analysis was carried out to demonstrate the existence of transcellular pathways in the stratum corneum, and does not imply that these transcellular pathways extend only to a depth of 3 μm.

CONFLICT OF INTEREST

The authors state no conflict of interest.

ACKNOWLEDGMENTS

This work was sponsored by the National Institutes of Health (EB000351), and by the US Army Research Office through the Institute for Soldier Nanotechnologies at MIT under Project 4.2: ''Non-invasive Diagnostics and Delivery of Injury Intervention Agents.'' The content of the information presented in this manuscript does not necessarily reflect the position or the policy of the US Government, and no official endorsement should be inferred.

REFERENCES

Alvarez-Román R, Merino G, Kalia YN, Naik A, Guy RH (2003) Skin permeability enhancement by low-frequency sonophoresis: lipid extraction and transport pathways. *J Pharm Sci* 92:1138–46

Bhatia KS, Gao S, Freeman TP, Singh J (1997) Effect of penetration enhancers and iontophoresis on the ultrastructure and cholecystokinin-8 permeability through porcine skin. *J Pharm Sci* 86:1011–5

Bodde HE, van der Brink I, Koerten HK, de Haan FHN (1991) Visualization of *in vitro* percutaneous penetration of mercuric chloride; transport through intercellular space versus cellular uptake through desmosomes. *J Control Release* 15:227–36

Bommannan D, Menon GK, Okuyama H, Elias PM, Guy RH (1992) Sonophoresis II: examination of the mechanism(s) of ultrasound-enhanced transdermal delivery. *Pharm Res* 9:1043–7

Bouwstra JA, de Graff A, Gooris GS, Nijsse J, Wiechers JW, van Aelst AC (2003) Water distribution and related morphology in human stratum corneum at different hydration levels. *J Invest Dermatol* 120:750–8

Denk W, Strickler JH, Webb WW (1990) Two-photon laser scanning fluorescence microscopy. *Science* 248:73–6

Diaspro A (1999) Introduction to two-photon microscopy. *Microsc Res Tech* 47:163–4

Elias PM (1996) The stratum corneum revisited. *J Dermatol* 23:756–8

Fartasch M, Schenetz E, Diepgen TL (1998) Characterization of detergent-induced barrier alterations – effect of barrier cream on irritation. *J Investig Dermatol Symp Proc* 3:121–7

Femenia-Fonta A, Balaguer-Fernandez C, Merino V, Rodilla V, Lopez-Castellano A (2005) Effect of chemical enhancers on the *in vitro* percutaneous absorption of sumatriptan succinate. *Eur J Pharm Biopharm* 61:50–5

Goffin V, Pierard-Franchimont C, Pierard GE (1999) Passive sustainable hydration of the stratum corneum following surfactant challenge. *Clin Exp Dermatol* 24:308–11

Johnson ME, Blankschtein D, Langer R (1997) Evaluation of solute permeation through the stratum corneum: lateral bilayer diffusion as the primary transport mechanism. *J Pharm Sci* 86:1162–72

Johnson ME, Mitragotri S, Patel A, Blankschtein D, Langer R (1996) Synergistic effects of chemical enhancers and therapeutic ultrasound on transdermal drug delivery. *J Pharm Sci* 85:670–8

Karande P, Mitragotri S (2002) High throughput screening of transdermal formulations. *Pharm Res* 19:655–60

Kushner J, Blankschtein D, Langer R (2004) Experimental demonstration of highly permeable localized transport regions in low-frequency sonophoresis. *J Pharm Sci* 93:2733–45

Magnusson BM, Runn P (1999) Effect of penetration enhancers on the permeation of the thyrotropin releasing hormone analogue pGlu-3-methyl-His-Pro amide through human epidermis. *Int J Pharm* 178:149–59

Masters BR, So PTC, Gratton E (1997) Multiphoton excitation fluorescence microscopy and spectroscopy of *in vivo* human skin. *Biophys J* 72:2405–12

Masters BR, So PTC, Gratton E (1998) Optical biopsy of *in vivo* human skin: multiphoton excitation microscopy. *Lasers Med Sci* 13:196–203

Menon GK, Bommannan DB, Elias PM (1994) High-frequency sonophoresis: permeation pathways and structural basis for enhanced permeability. *Skin Pharmacol* 7:130–9

Menon GK, Elias PM (1997) Morphological basis for a pore-pathway in mammalian stratum corneum. *Skin Pharmacol* 10:235–46

Mitragotri S, Ray D, Farrell J, Tang H, Yu B, Kost J *et al.* (2000) Synergistic effect of low-frequency ultrasound and sodium lauryl sulfate on transdermal transport. *J Pharm Sci* 7:892–900

Miyazawa K, Ogawa M, Mitsui T (1984) The physico-chemical properties and protein denaturation potential of surfactant mixtures. *Int J Cosmet Sci* 6:33–46

Mizushima J, Kawasaki Y, Tabohashi T, Kitano T, Sakamoto K, Kawashima M *et al.* (2000) Effect of surfactants on human stratum corneum: electron paramagnetic resonance study. *Int J Pharm* 197:193–202

Montaga W, Klingman AM, Carlisle KS (1992) *Atlas of normal human skin*. New York: Springer-Verlag

Montgomery DC, Runger GC, Hubele NF (1998) *Engineering statistics*. New York: John Wiley & Sons, Inc

Na R, Stender I-M, Ma L, Wulf HC (2000) Auto-fluorescence spectrum of the skin: component bands and body site variations. *Skin Res Technol* 6:112–7

Na R, Stender I-M, Ma L, Wulf HC (2001) Auto-fluorescence of human skin is age-related after correction for skin pigmentation and redness. *J Invest Dermatol* 116:536–40

Paliwal S, Menon GK, Mitragotri S (2006) Low-frequency sonophoresis: ultrastructural basis for stratum corneum permeability assessed using quantum dots. *J Invest Dermatol* 126:1095–101

Peck KD, Ghanem AH, Higuchi WI (1994) Hindered diffusion of polar molecules through and effective pore radii estimates of intact and ethanol treated human epidermal membrane. *Pharm Res* 11:1306–14

Periasamy A, Skoglund P, Noakes C, Keller R (1999) An evaluation of two-photon excitation versus confocal and digital deconvolution fluorescence microscopy imaging in xenopus morphogenesis. *Microsc Res Tech* 47:172–81

Pillai O, Nair V, Panchagnula R (2004) Transdermal iontophoresis of insulin: IV. Influence of chemical enhancers. *Int J Pharm* 269:109–20

Rhein LD, Robbins CR, Ferne K, Cantore R (1986) Surfactant structure effects on swelling of isolated human stratum corneum. *J Soc Cosmet Chem* 37:125–39

Schaefer H, Redelmeier TE (1996) *Skin barrier*. New York: Karger

Soeller C, Cannell MB (1999) Two-photon microscopy: imaging in scattering samples and three dimensionally resolved flash photolysis. *Microsc Res Tech* 47:182–95

Tang H, Blankschtein D, Langer R (2002a) Effects of low-frequency ultrasound on the transdermal permeation of mannitol: comparative studies with *in vivo* and *in vitro* skin. *J Pharm Sci* 91:1776–94

Tang H, Mitragotri S, Blankschtein D, Langer R (2001) Theoretical description of transdermal transport of hydrophilic permeants: application to low-frequency sonophoresis. *J Pharm Sci* 90:545–68

Tang H, Wang CCJ, Blankschtein D, Langer R (2002b) An investigation of the role of cavitation in low-frequency ultrasound-mediated transdermal drug transport. *Pharm Res* 19:1160–9

Tezel A, Mitragotri S (2003) Interactions of inertial cavitation bubbles with stratum corneum lipid bilayers during low-frequency sonophoresis. *Biophys J* 85:3502–12

Tezel A, Sens A, Mitragotri S (2002a) A theoretical analysis of low-frequency sonophoresis: dependence of transdermal transport pathways on frequency and energy density. *Pharm Res* 19:1841–6

Tezel A, Sens A, Mitragotri S (2002b) Investigations of the role of cavitation in low-frequency sonophoresis using acoustic spectroscopy. *J Pharm Sci* 91:444–53

Uhoda E, Leveque JL, Pierard GE (2005) Silicon image sensor technology for *in vivo* detection of surfactant-induced corneocyte swelling and drying. *Dermatology* 210:184–8

Wells PNT (1977) *Biomedical applications of ultrasound*. New York: Plenum Press

Welzel J, Metker C, Wolff HH, Wilhelm KP (1998) SLS-irritated human skin shows no correlation between degree of proliferation and TEWL increase. *Arch Dermatol Res* 290:615–20

Wilhelm KP, Cua AB, Wolff HH, Maibach HI (1993) Surfactant-induced stratum corneum hydration *in vivo*: prediction of the irritation potential of anionic surfactants. *J Invest Dermatol* 101:310–5

Xhauflaire-Uhoda E, Loussouarn G, Haubrechts C, Saint Leger D, Pierard GE (2006) Skin capacitance imaging and corneosurfametry: a comparative assessment of the impact of surfactants on the stratum corneum. *Contact Dermatitis* 54:249–53

Yamashita N, Tachibana K, Ogawa K, Tsujita N, Tomita A (1997) Scanning electron microscopic evaluation on the skin surface after ultrasound exposure. *The Anatomical Record* 247:455–61

Yu B, Dong C, So PTC, Blankschtein D, Langer R (2001) *In vitro* visualization and quantification of oleic acid induced changes in transdermal transport using two-photon fluorescence microscopy. *J Invest Dermatol* 117:16–25

Yu B, Kim KH, So PTC, Blankschtein D, Langer R (2002) Topographic heterogeneity in transdermal transport revealed by high-speed two-photon microscopy: determination of representative skin sample sizes. *J Invest Dermatol* 118:1085–8

Yu B, Kim KH, So PTC, Blankschtein D, Langer R (2003a) Visualization of oleic acid-induced transdermal diffusion pathways using two-photon fluorescence microscopy. *J Invest Dermatol* 120:448–55

Yu B, Kim KH, So PTC, Blankschtein D, Langer R (2003b) Evaluation of fluorescent probe surface intensities as an indicator of transdermal permeant distributions using wide-area two-photon fluorescence microscopy. *J Pharm Sci* 92:2354–65